Int. J. Heat Mass Transfer. Vol. 16, pp. 2407–2420. Pergamon Press 1973. Printed in Great Britain

TRANSIENT HEAT TRANSFER IN BÉNARD CONVECTION

R. C. NIELSEN* and R. H. SABERSKY

Division of Engineering and Applied Science, California Institute of Technology, Pasadena, California, U.S.A.

(*Received* 15 *September* 1972 *and in revised form* 14 *March* 1973)

Abstract—Experimental results are presented for a study of the effects of time-dependent heating on Bénard convection, where the fluids were 5cs (centistoke), 100cs and 500cs viscosity grades of silicone oil. Fluid layer depths were 0·00635 m, 0·01270 m and 0·01905 m. For each run the heat flux at the lower surface was approximately constant, and in the several runs a range of fluxes from $9{\cdot}2 \times 10^2$ to $1{\cdot}9 \times 10^7$ (in dimensionless terms) was covered. The experiments were designed to examine the effects of different heating rates on the onset of convection, on the change of the Rayleigh number with time and on the development of motion. Observations were made from shadowgraph images, which were recorded photographically. As the heat flux at the lower surface is increased, the temperature difference required for the initiation of convection increases while the time to the onset of motion decreases. For the conditions of the present tests a "closed cell" pattern is the first to be observed, shortly after the onset of motion. This pattern does not appear in the steady-state system. Because of the "large" (greater than about 100) Prandtl number, specifying the time and the lower surface heat flux is sufficient to characterize the state of the fluid layer.

NOMENCLATURE

- c_p, specific heat at constant pressure [$\mathrm{J kg^{-1} K^{-1}}$];
- d, fluid layer depth [m];
- g, acceleration of gravity [$9{\cdot}807\ \mathrm{m^2 s^{-1}}$];
- H, heating rate, lower surface heat flux ($g\beta d^4 Q/\varkappa\nu k$) [dimensionless];
- k, thermal conductivity [$\mathrm{W m^{-1} K^{-1}}$];
- Nu, Nusselt number (H/Ra) [dimensionless];
- Pr, Prandtl number ($\nu/\varkappa$) [dimensionless];
- Q, heating rate, lower surface heat flux [$\mathrm{W m^{-2}}$];
- Ra, Rayleigh number ($g\beta d^3 \Delta T/\varkappa\nu$) [dimensionless];
- t, elapsed time from start of experimental run [s];
- T, temperature in the fluid at various elevations [K];
- z, vertical distance from the lower surface of the fluid layer [m];
- β, coefficient of volume thermal expansion [$\mathrm{K^{-1}}$];
- ΔT, temperature difference between the lower and upper surfaces of the fluid layer [K];
- $\varkappa$, thermal diffusivity [$\mathrm{m^2 s^{-1}}$];
- ν, kinematic viscosity [$\mathrm{m^2 s^{-1}}$];
- ρ, density [$\mathrm{kg m^{-3}}$];
- τ, elapsed time from start of experimental run [$t\varkappa/d^2$] [dimensionless].

Subscript

- cr, value of a parameter at the onset of motion.

* Presently at J T Thorpe Inc., Los Angeles, California, U.S.A.

INTRODUCTION

THE HEATING of a horizontal fluid layer from below has been studied extensively from the beginning of this century when Bénard [1] published the results of his experiments on such a system. His name is now generally associated with this type of convection. Part of the interest in the Bénard problem may be explained by the fact that many and diverse natural phenomena are related to Bénard convection, for example, the motion of certain atmospheric layers, the

movements in the earth mantle giving rise to sea floor spreading and plate tectonics, as well as the heat transfer inside rooms and in cooking vessels. Aside from these applied aspects, however, the Bénard problem is a most intriguing one from a mathematical point of view. The nonlinear governing equations and the selection of the preferred solution offer a great challenge to the theoretician. The present work was stimulated because of a desire to explain certain cellular flow patterns which seemed to occur in the heat transfer to fluids with strongly varying properties, in particular fluids near the critical point. It was thought that the patterns might also have been influenced by time dependent, transient heating. To obtain a better understanding of this phenomenon it was decided to study first the convection of a system with relatively constant properties, with emphasis on the effect of transient heating.

PREVIOUS STUDIES

For the reasons just mentioned a large amount of research has been devoted to the problem under consideration and a very extensive literature on the subject exists. The progress in the field has been surveyed periodically and among the principal publications of this type are those by Chandrasekhar [2], Segel [3] and Brindley [4]. The studies most pertinent for the present work are those concerned with the experimental investigation of the transient behavior of a fluid layer when heated from below.

The first experimental work specifically studying the effect of time dependency on the initiation of convection was that of Soberman [5]. His experiments approximated the case of constant heat flux at the lower surface for an initially isothermal system. He found that rapid heating did indeed affect the critical Rayleigh number. As the dimensionless heating rate, H, was increased beyond that required to initiate steady-state convection, the critical Rayleigh number was increased with the data falling on the curve $Ra_{cr} = 90{\cdot}7\,H^{(0{\cdot}394)}$.

Spangenberg and Rowland [6] used a layer of water in which the top surface was free to evaporate. They found that the upper surface temperature decreased approximately linearly until convection was initiated. The critical Rayleigh number was determined to be 1193. Similar experiments were carried out by Foster [7] over a wider range of parameters. In some more recent work Foster [8] used deep layers (greater than 0·05 m) of water and silicone oil to study the length of time required for the initiation of convection for the analogous problem of linearly increasing lower surface temperature.

Several experimental works have been published using time-dependent density gradients which were created by solute concentrations instead of temperature differences. The works are generally analogous to the case of a step increase of the lower surface temperature. These papers include those of Blair and Quinn [9], Mahler and Schechter [10], and Plevan and Quinn [11].

Onat and Grigull [12] reported results for deep layers of several different working fluids when the lower surface was subjected to constant heat flux.

In a quite different form of heating, that of increasing or decreasing the two surface temperatures at the same constant rates, Krishnamurti [13, 14] reported data on changes in the critical Rayleigh number, critical wave number, planform shape and heat transfer. Recently, Busse and Whitehead [15] published data and photographs on the evolution of instabilities which initially were in the form of two dimensional rolls. In these experiments a technique was used to favor the development of rolls of a particular wave number, and the influence of the initial wave number and the Rayleigh number of this development was investigated. The stability problem has also been treated theoretically by a number of authors: among the earliest were Goldstein [16], Currie [17] and Foster [18].

Finally there is a very interesting set of experiments by Hahne [19] in which the fluid was CO_2 near its critical point. As the property

variations are of major importance in this case, the subject matter of this paper is, somewhat outside of the immediate scope of the present study.

EXPERIMENTAL INSTALLATION

The experiments performed as part of this research were designed to determine the effects of time-dependent heating on Bénard convection. Important information to be determined included the temperatures of the two bounding surfaces, the amount of heat conducted through the lower boundary into the fluid layer, and an optical determination of the onset of convection and the patterns of motion once convection was initiated. It was decided to use the shadowgraph technique for visualization and to view the flow field from above. This required the upper boundary of the fluid layer to be a transparent material.

These considerations led to the design of a chamber as shown in Fig. 1. The bottom of the chamber was formed by a layer of laminated phenolic plastic 0·2318 m ($9\frac{1}{8}$ in.) square by 0·0381 m ($1\frac{1}{2}$ in.) thick. Fastened to this base was a glass plate 0·2286 m (9 in.) square by 0·00635 m ($\frac{1}{4}$ in.) thick. The upper surface of the glass had a metallic oxide coating bonded to it. This coating was used as the heater. The upper surface of the fluid layer was formed by an identical piece of glass with the coating on the lower surface. Sets of plastic dowels were used to obtain the desired spacing of the plates which in turn determined the depths of the fluid layers. Experiments were conducted with three different depths of 0·00635 m ($\frac{1}{4}$ in.), 0·01270 m ($\frac{1}{2}$ in.) and 0·01905 m ($\frac{3}{4}$ in.).

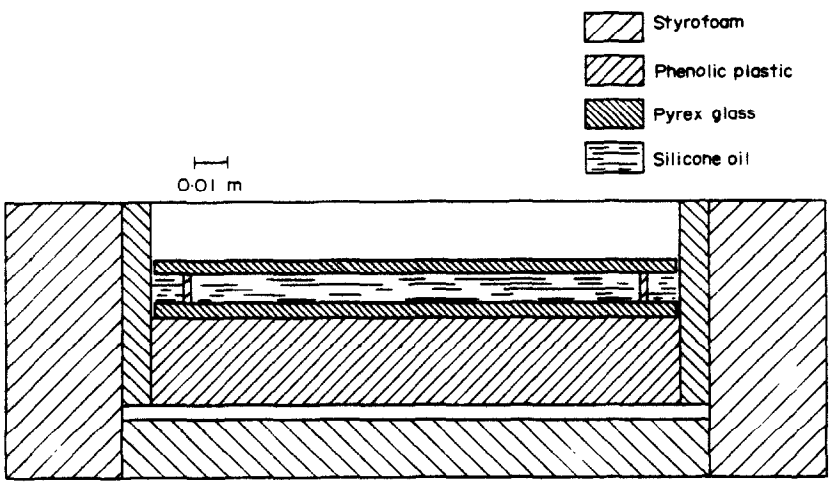

FIG. 1. Experimental apparatus in cross-section.

Heating of the fluid layer was accomplished conducting a direct current through the metallic oxide coating on the lower glass plate. Heat flow through the base of the apparatus was monitored by a heat flux meter, manufactured by Hy-Cal Engineering. The temperatures of the bounding surfaces were determined by measuring the changes of resistance of the two glass coatings. Because the resistance changes were small, Wheatstone bridges were used with the plates as one of the legs. The changes were determined by detecting the imbalance of the bridges. The changes in resistance were converted to changes in temperature by calibration constants for each plate that had been determined from measurements in a constant temperature bath.

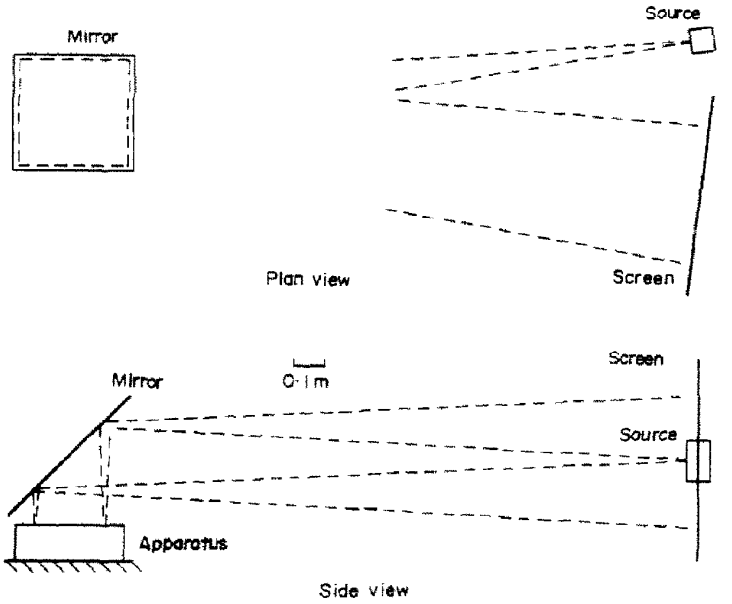

FIG. 2. Schematic drawing of the shadowgraph optics.

A diagram of the lighting arrangement is shown in Fig. 2. Light from a point source was reflected from a front surface mirror located above the chamber through the fluid layer to a mirror which was located on the back side of the lower glass surface. From this mirror the light was again reflected through the fluid layer to the front surface mirror. Because the light source was slightly off axis, an image was formed on the screen of flashed opal glass located adjacent to the lamp. The dark regions indicate relatively high temperatures and the colder regions appear as bright areas.

Silicone oils with viscosities of 5cs, 100cs and 500cs were used as working fluids. The viscosity, density and thermal coefficient of expansion were measured as a function of temperature for each of the oils while the thermal conductivities and specific heats were taken from the available literature (see Nielsen [20] for details). The values of the physical properties at 25 C are given in Table 1.

EXPERIMENTAL RESULTS

(a) *Experimental procedure*

The experimental work was concerned with two aspects of the effects of time-dependent heating on Bénard convection: first, the onset of instability and second, the behavior of the system during the transient phase subsequent to the onset of instability.

Table 1. Property values of silicone oils at 25 C

Grade	ν ($m^2 s^{-1} \times 10^6$)	ρ (kgm^{-3})	β ($K^{-1} \times 10^3$)	k ($Wm^{-1} K^{-1}$)	c_p ($Jkg^{-1} K^{-1}$)	$\varkappa$ ($m^2 s^{-1} \times 10^6$)	Pr
5·0	3·86	913·7	0·987	0·1215	1549	0·0858	45·0
100	100	963·9	0·890	0·1585	1473	0·1116	896
500	523	969·1	0·958	0·1623	1532	0·1093	4770

For a given oil and a given depth a typical experimental run started by presetting the external resistance in the electrical loop of the lower plate so as to fix the heating rate. A small current was run through the coating of the upper plate to monitor the change of resistance. Heating was started with an initially isothermal system and the temperatures of the plates were recorded as a function of time. The time at which motion was detected on the shadowgraph image was also noted. Once motion was initiated photographs of the developing flow patterns were taken. The continuous electrical outputs were translated to digital form and, using an IBM 360 computer, were converted to the required temperatures and heat fluxes as well as the appropriate dimensionless parameters such as the Rayleigh number, the dimensionless heat flux at the lower surface, and the dimensionless time. Physical properties were evaluated at the instantaneous arithmetic average of the surface temperatures.

(b) *Onset of instability*

The onset of instability was established as that time at which motion was first observed on the shadowgraph. The time from the start of heating to this initiation of convection, called the critical time, is given in dimensionless form as

$$\tau_{cr} = \frac{t_{cr}\kappa}{d^2}.$$

The experimental results at the onset of instability are presented in terms of the Rayleigh number

$$Ra_{cr} = \frac{g\beta d^3 \Delta T_{cr}}{\kappa\nu}$$

the dimensionless heat flux at the lower surface

$$H = \frac{g\beta d^4 Q}{\kappa\nu k}$$

and the Nusselt numbers based on this heat flux

$$Nu_{cr} = -\frac{d}{\Delta T_{cr}}\left(\frac{\partial T}{\partial z}\right)_{0,cr} \equiv \frac{H}{Ra_{cr}}.$$

The range of experimental parameters is given in Table 2.

In Fig. 3 the results are shown in a graph of the critical time vs the heating rate (both in dimensionless terms). It is seen that the critical time

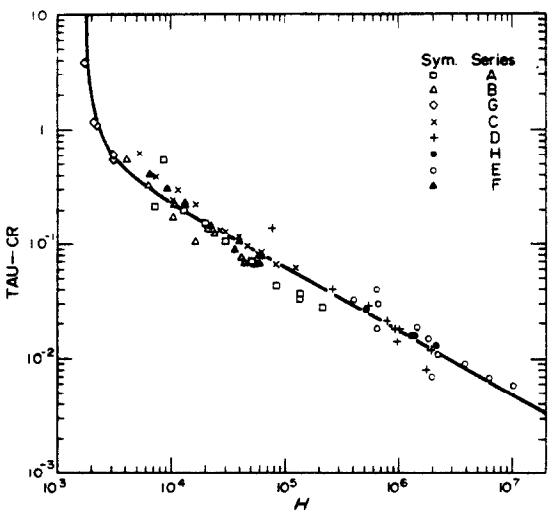

FIG. 3. Critical time as a function of the heating rate.

Table 2. Range of parameters for experimental runs

Series	No. runs	Oil grade	Depth (m)	τ_{cr}	H	Ra_{cr}
A	12	100	0·01905	0·028–0·553	$8{\cdot}73 \times 10^3$–$2{\cdot}13 \times 10^5$	$5{\cdot}53 \times 10^3$–$3{\cdot}80 \times 10^4$
B	8	100	0·01270	0·069–0·553	$4{\cdot}11 \times 10^3$–$4{\cdot}40 \times 10^4$	$2{\cdot}16 \times 10^3$–$1{\cdot}21 \times 10^4$
G	6	100	0·00635	0·552–3·86	$1{\cdot}74 \times 10^3$–$3{\cdot}17 \times 10^3$	$1{\cdot}43 \times 10^3$–$1{\cdot}85 \times 10^3$
F	9	500	0·01905	0·066–0·407	$6{\cdot}58 \times 10^3$–$5{\cdot}99 \times 10^4$	$4{\cdot}12 \times 10^3$–$1{\cdot}34 \times 10^4$
E	12	5	0·01905	0·005–0·040	$6{\cdot}45 \times 10^5$–$9{\cdot}94 \times 10^6$	$5{\cdot}93 \times 10^4$–$6{\cdot}34 \times 10^5$
D + H	14	5	0·01270	0·005–0·138	$7{\cdot}75 \times 10^4$–$2{\cdot}01 \times 10^6$	$2{\cdot}60 \times 10^4$–$1{\cdot}92 \times 10^5$
C	14	5	0·00635	0·064–0·618	$5{\cdot}28 \times 10^3$–$8{\cdot}23 \times 10^4$	$2{\cdot}90 \times 10^3$–$2{\cdot}71 \times 10^4$

decreases as the heating rate is increased. As the heating rate decreases, on the other hand, the critical time increases rapidly; this is to be expected as the system is *stable* for very low heating rates, which means that the critical time will have to go towards infinity when the heating rate falls below the limiting value which can cause convective motion. For very high heating rates instability is likely to occur before the effects of heating have penetrated the fluid layer to the full depth. The depth, therefore, should no longer have an influence on the critical time. As the dimensionless time is proportional to d^2 and the dimensionless heat transfer rate proportional to d^4, it is necessary, in order to satisfy this condition, that the critical time be inversely proportional to the square root of the heating rate for large values of that rate. As can be seen from Fig. 3, the shape of the curve tends towards such a value.

Figure 4 represents a plot of the critical Rayleigh number vs dimensionless heat flux at the lower surface. As the heat flux increases the critical Rayleigh number increases. Following arguments similar to those presented above, for high heating rates Ra_{cr} should be proportioned to $H^{\frac{1}{4}}$. The trend of the data indicates this kind of relationship.

In Fig. 5 the critical Nusselt number (a measure of heat transfer coefficient) is plotted against the critical Rayleigh number (a measure of the buoyancy forces relative to the viscous forces). The data again apply to the onset of the convective motion. As high critical Rayleigh numbers correspond to high heat transfer rates, one may again argue that the relation between the Nusselt number and the critical Rayleigh number should become independent of the depth of the layer, d. This independence would require that Nu_{cr} be proportional to $(Ra)^{\frac{1}{3}}$. As indicated in Fig. 5, the curve does approach this slope as expected. A plot of the critical time shown as a parametric function of critical Rayleigh numbers and dimensionless heat flux at the lower surface is presented in Fig. 6.

Taken together, the four graphs indicate that

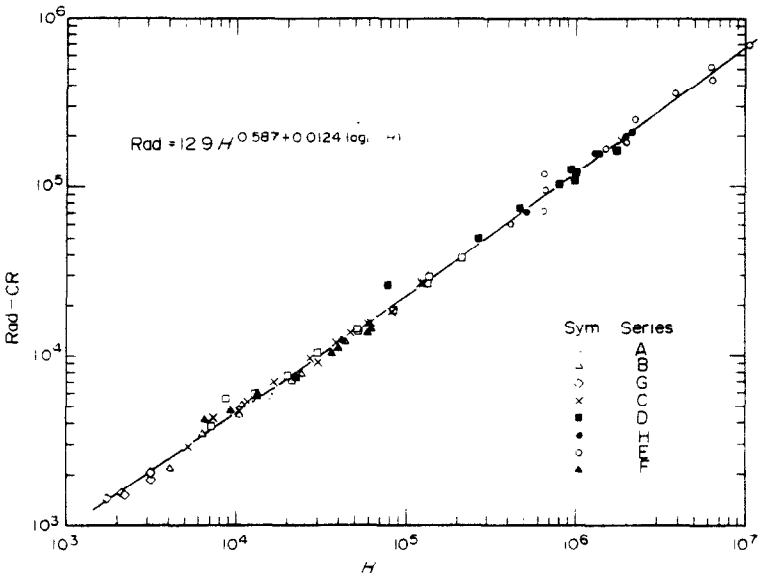

FIG. 4. Rayleigh number at the onset of motion vs the lower surface heat flux.

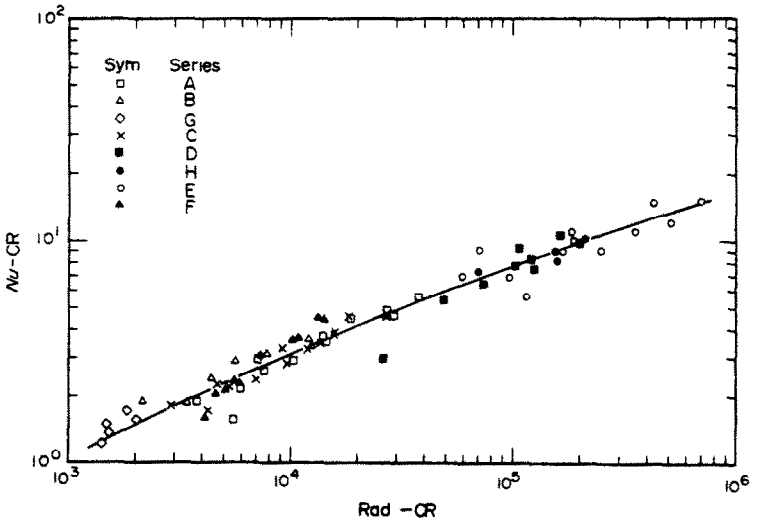

FIG. 5. Critical Nusselt number vs critical Rayleigh number.

as the rate of heating is increased (a) the time to the start of the convective motion decreases; (b) the critical Nusselt number and the critical Rayleigh number increase; and (c) the change in these parameters is such that the actual temperature difference at the critical time for a given depth and fluid increases with higher heating rates.

These trends are in agreement with theoretical predictions, for example, those of Currie [17]

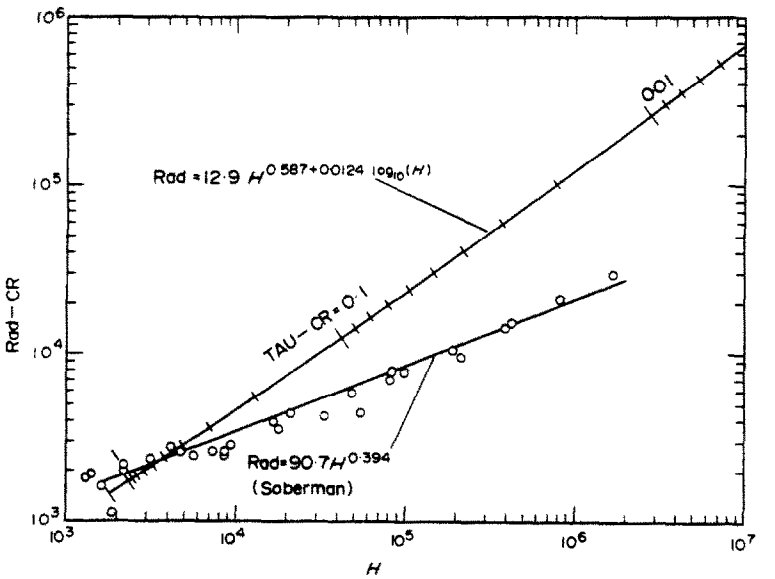

FIG. 6. Critical time as a function of critical Rayleigh number and the heating rate. Comparison of present results with results of Soberman [5].

and Foster [18]. However, the values of the analytically predicted times are significantly shorter than those observed. The probable explanation for this difference is that the analytical work is concerned with the instant at which an initial disturbance can begin to grow, whereas the first visual evidence will correspond to a disturbance which already has had a period of growth.

The present results may also be compared to the experimental work of Soberman [5] (see Fig. 6), and it is seen that the data from those experiments are considerably lower. It is believed that the difference is brought about by an assumption Soberman made in extrapolating the temperature profile for the purpose of determining the overall differential across the two plates. This point was first mentioned by Currie [17]. A more precise description of the profile would probably lead to much better agreement with the present results.

(c) *Transient convection*

The transient convection period is defined as that extending from the onset of convection to the establishment of steady state conditions. The experimental data were collected first in the form of a series of graphs of the instantaneous Rayleigh number as a function of the heating rate. Each graph is for a specified value of the dimensionless time, τ, and each data point corresponds to a separate experiment. Two typical graphs are reproduced in Fig. 7 ($\tau = 0{\cdot}10$) and Fig. 8 ($\tau = 0{\cdot}20$). On the basis of this information a composite diagram was then prepared (Fig. 9) in which the Nusselt number is plotted against Rayleigh number for constant values of the dimensionless time. In addition lines of constant lower-surface-heat-flux are indicated, and the chronological progress of an individual experiment can be traced approximately by following one of these lines in a direction from the upper left to the lower right, i.e. in a direction of increasing time. As an example, consider the constant heating line $H = 10^5$. At times $\tau = 0{\cdot}01$, $0{\cdot}05$ and up to about $0{\cdot}07$, heat transfer through the liquid layer is by conduction only. As the constant H line crosses the upper dashed line (marked TAU = TAU–CR) the fluid becomes unstable, i.e. convection begins. The convection patterns

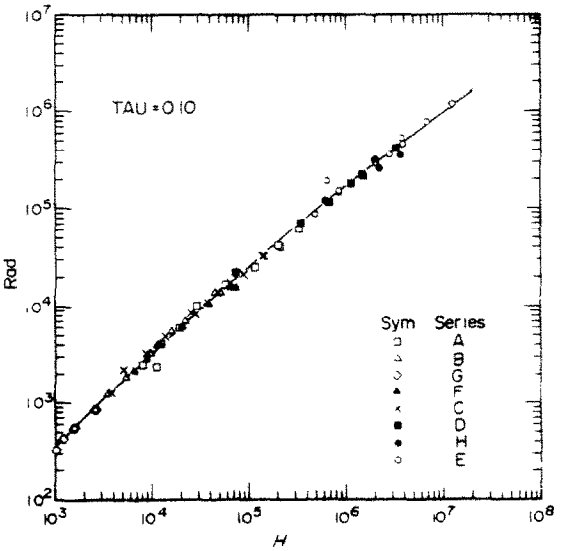

FIG. 7. Rayleigh number vs the heating rate at $\tau = 0{\cdot}10$.

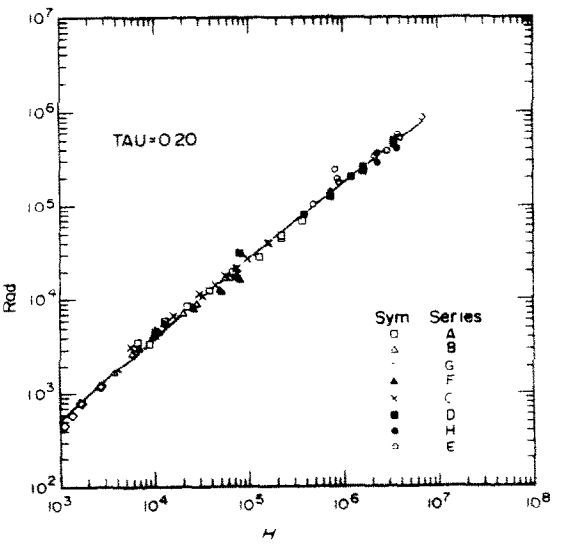

FIG. 8. Rayleigh number vs the heating rate at $\tau = 0{\cdot}20$.

then develops gradually, and in the present examples the final pattern as well as the asymptotic values of Nu and Ra are reached at a time approximately equal to $\tau = 1{\cdot}30$.

which the data in this region may be compared. As can be seen from the figure, the higher the heating rates (and the higher the Rayleigh numbers) the larger the possible deviations from

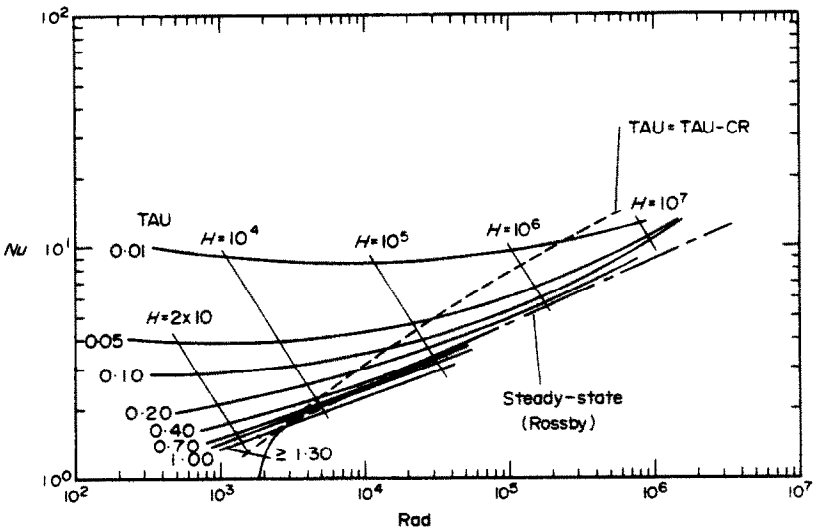

FIG. 9. Nusselt number vs the Rayleigh number for $\tau = 0{\cdot}01, 0{\cdot}05, 0{\cdot}10, 0{\cdot}20, 0{\cdot}40, 0{\cdot}70, 1{\cdot}00 \geqslant 1{\cdot}30$ with lines of constant lower surface heat flux and results for $\tau = \tau_{cr}$ and results of Rossby [21].

Also shown in Fig. 9 is a dashed curve corresponding to the steady state values of Nu and Ra as determined by Rossby [21]. As can be seen from the graph, the asymptotic value of the foregoing example lies about 10 per cent below that found by Rossby. Such a deviation is quite within the accuracy of the experimental data. The results of Rossby's who made a very extensive investigation of the steady state condition, may, therefore, be used as a proper indication of the steady state limit for the present experiments.

As mentioned earlier, the present study was concerned principally with the period from the time of onset of convection to the time at which steady state conditions were approached. The region is indicated by the two dashed lines ("TAU = TAU–CR", and "steady state") in Fig. 9 and there is little prior information to the steady state values. For $H = 10^6$, for example, the Nusselt number at the onset of motion is approximately 50 per cent above the steady state value.

(d) *Visual studies*

The apparatus was designed to allow observation of the flow pattern by means of shadowgraph illumination (see Sec. 3). It was possible to discern certain general types of flow patterns and the development of the flow will be described in terms of these patterns.

All flow observations were made from above and photographic records were taken at selected intervals. It was found that the flow field could be described in terms of several plan forms designated as "closed cells", "cylindrical rolls", "vermiculated rolls", and "polygonal cells". The "closed cells" refers to a flow in which a

small column of warm fluid rises causing the surrounding cold fluid to move downward: each cell appears to be fairly separate from the other. An example of a "closed cell" pattern is shown in Fig. 10a. "Cylindrical rolls" are shown in Fig. 10b, and it is seen that the axes of the rolls are not always straight nor are they always parallel to each other. When the curvature and orientation of the rolls becomes more random, the term "vermiculate" (which was coined by Avsec [22]) has been used to describe the "worm-like" appearance as seen in Fig. 10c. An example of a "polygonal-cell" pattern is given in Fig. 10d. The motion in these cells is certainly three-dimensional in nature and at the higher Rayleigh number it will be unsteady, giving more and more the appearance of a turbulent flow (Fig. 10e).

The photographs are grouped according to the plate spacing at which they were taken. Let us examine first several sequences taken for a plate spacing of $\frac{1}{4}$ in. The record shown in Fig. 11 was obtained at a relatively low heating rate ($H \approx 3{\cdot}2 \times 10^3$) and the resulting Rayleigh numbers are consequently also low ($Ra = 2{\cdot}0 \times 10^3$ at end of run). The first photograph shows fairly well the characteristic dot-like appearance which is associated with the "closed cell" pattern. This pattern is peculiar to the transient phase and has not been observed for any steady-state conditions. In the present sequence the dots—or "closed-cells"—are seen to merge until in the last photograph of the run a "roll-like" pattern begins to be discernible. At a high heat transfer rate for the same spacing ($H \approx 8{\cdot}3 \times 10^4$, $Ra = 3{\cdot}89 \times 10^4$—Fig. 12) the first photograph again shows the closed-cell pattern. This pattern now turns into one exhibiting "vermiculate" rolls. Finally the pattern of these rolls is modified further by what appears to be a secondary cellular flow indicated by very light colour lines. This cellular flow may be regarded as a precursor of the three-dimensional polygonal patterns which are seen at the Rayleigh numbers obtainable with the wide plate spacings.

The next series is for a plate spacing of $\frac{1}{2}$ in., which leads to generally higher dimensionless heating rates and higher Rayleigh numbers. The sequence in Fig. 13 was taken at $H \approx 1{\cdot}6 \times 10^4$ and the final Rayleigh number is $8{\cdot}5 \times 10^3$. Again the first pattern to emerge is that of the dot-like "closed cells", and the subsequent pictures show how these dots develop step by step into a roll-like pattern. The roll spacing is about double that for the first series, which is consistent as the latter was taken at half the plate spacing. One also has to note, however, that for the given Rayleigh number, the rolls in the $\frac{1}{4}$ in. gap series already had assumed the curved "vermiculate" shape. As the wider gap brings about a lower l/d ratio, it is probable that the side walls are responsible for maintaining the alignment of the rolls for somewhat larger Rayleigh numbers. At a higher heating rate ($H \approx 4{\cdot}7 \times 10^5$—Fig. 14) the initial dot-like pattern branches out in several directions leading to a cellular pattern. In addition, a secondary flow structure within each cell may be noticed, which is indicated by very light coloured boundaries. The development at a still higher heating rate is shown in Fig. 15 ($H \approx 1{\cdot}4 \times 10^6$). Again the initial dot-like pattern of closed cells is clearly exhibited. The development of vermiculate rolls does not seem to occur and the flow changes directly into a pattern of irregular cells which is maintained as the steady-state heat-transfer conditions are approached. The flow within the cells now appears turbulent.

The widest plate spacing used was $\frac{3}{4}$in. This reduces the length to depth ratio of the fluid layer to 10·3, and the sidewalls will now exert a more definite influence on the flow pattern. At a relatively low heating rate ($H \approx 1{\cdot}3 \times 10^4$—Fig. 16) the dot-like pattern of closed cells again develops and changes into two-dimensional rolls, as for the experiments at the smaller gap spacing (Figs. 17 and 18). As the dimensionless parameters H and Ra are similar one would expect the roll width and spacing to increase with the gap size and this trend is clearly evident.

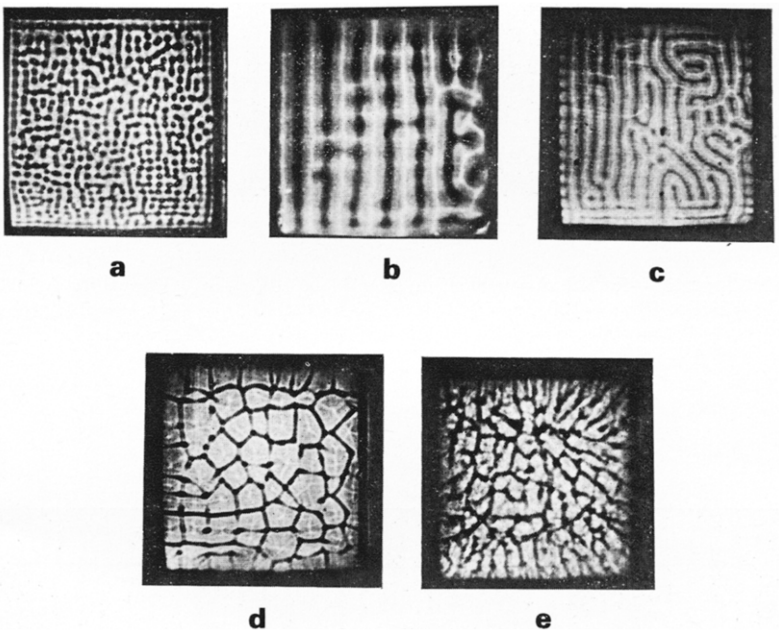

FIG. 10. Typical flow patterns: (a) "Closed cell" pattern— 5cs Oil, $d = 0{\cdot}00635$ m, $H \approx 1{\cdot}3 \times 10^5$, $\tau_{cr} = 0{\cdot}064$, $Ra = 3{\cdot}29 \times 10^4$, $t = 50$ s, $\tau = 0{\cdot}11$; (b) "Cylindrical roll pattern"— 100cs Oil, $d = 0{\cdot}01270$ m, $H \approx 1{\cdot}1 \times 10^4$, $\tau_{cr} = 0{\cdot}173$, $Ra = 5{\cdot}43 \times 10^3$, $t = 1070$ s, $\tau = 0{\cdot}739$; (c) "Vermiculated roll" pattern—5cs Oil, $d = 0{\cdot}00635$ m, $H \approx 1{\cdot}7 \times 10^4$, $\tau_{cr} = 0{\cdot}223$, $Ra = 1{\cdot}05 \times 10^4$, $t = 965$ s, $\tau = 2{\cdot}06$; (d) "Polygonal cell" patterns—5cs Oil, $d = 0{\cdot}01270$ m, $H \approx 4{\cdot}7 \times 10^5$, $\tau_{cr} = 0{\cdot}029$, $Ra = 1{\cdot}30 \times 10^5$, $t = 420$ s, $\tau = 0{\cdot}224$; (e) "Turbulent flow" pattern—5cs Oil, $d = 0{\cdot}01905$ m, $H \approx 1{\cdot}1 \times 10^7$, $\tau_{cr} = 0{\cdot}006$, $Ra = 1{\cdot}76 \times 10^6$, $t = 595$ s, $\tau = 0{\cdot}140$.

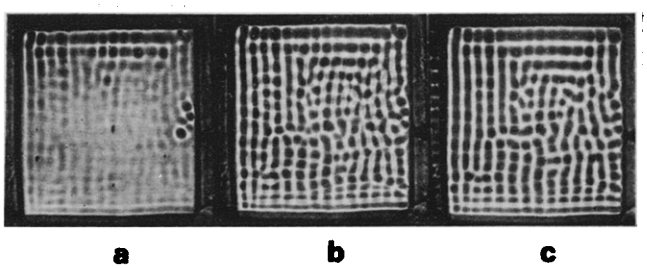

FIG. 11. "Low heating rate"—100cs Oil, $d = 0{\cdot}00635$ m, $H \approx 3{\cdot}2 \times 10^3$, $\tau_{cr} = 0{\cdot}552$: (a) $Ra = 2{\cdot}09 \times 10^3$, $t = 310$ s, $\tau = 0{\cdot}86$; (b) $Ra = 2{\cdot}12 \times 10^3$, $t = 415$ s, $\tau = 1{\cdot}14$; (c) $Ra = 2{\cdot}00 \times 10^3$, $t = 685$ s, $\tau = 1{\cdot}89$.

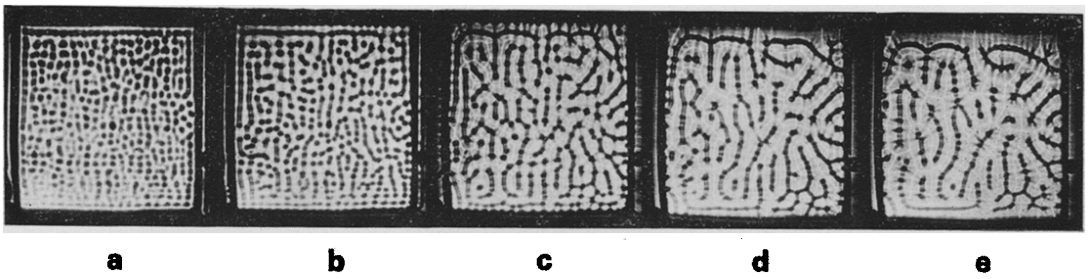

FIG. 12. "High heating rate"—5cs Oil, $d = 0{\cdot}00635$ m, $H \approx 8{\cdot}3 \times 10^4$, $\tau_{cr} = 0{\cdot}068$: (a) $Ra = 2{\cdot}06 \times 10^4$, $t = 45$ s, $\tau = 0{\cdot}10$; (b) $Ra = 2{\cdot}77 \times 10^4$, $t = 100$ s, $\tau = 0{\cdot}21$; (c) $Ra = 3{\cdot}40 \times 10^4$, $t = 245$ s, $\tau = 0{\cdot}52$; (d) $Ra = 3{\cdot}69 \times 10^4$, $t = 400$ s, $\tau = 0{\cdot}85$; (e) $Ra = 3{\cdot}89 \times 10^4$, $t = 610$ s, $\tau = 1{\cdot}30$.

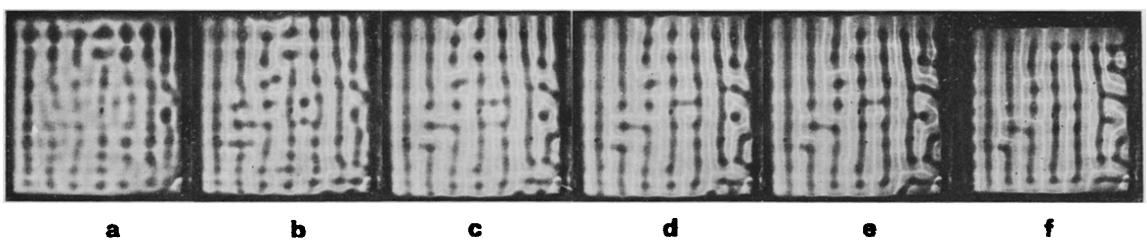

FIG. 13. "Intermediate heating rate"—100cs Oil, $d = 0{\cdot}01270$ m, $H \approx 1{\cdot}6 \times 10^4$, $\tau_{cr} = 0{\cdot}104$: (a) $Ra = 7{\cdot}02 \times 10^3$, $t = 260$ s, $\tau = 0{\cdot}180$; (b) $Ra = 7{\cdot}55 \times 10^3$, $t = 380$ s, $\tau = 0{\cdot}263$; (c) $Ra = 7{\cdot}83 \times 10^3$, $t = 660$ s, $\tau = 0{\cdot}456$; (d) $Ra = 8{\cdot}17 \times 10^3$, $t = 800$ s, $\tau = 0{\cdot}553$; (e) $Ra = 8{\cdot}37 \times 10^3$, $t = 960$s, $\tau = 0{\cdot}663$; (f) $Ra = 8{\cdot}5 \times 10^3$, $t = 1230$ s, $\tau = 0{\cdot}950$.

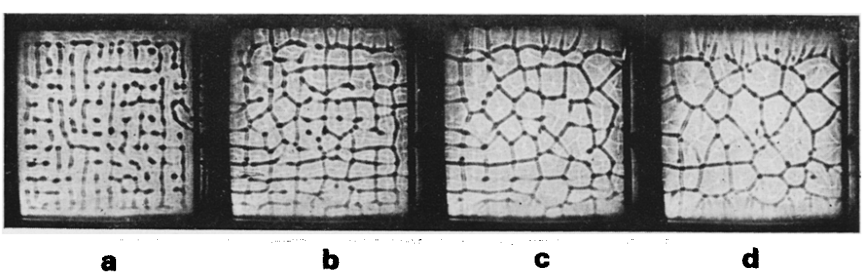

FIG. 14. "High heating rate"—5cs Oil, $d = 0{\cdot}01270$ m, $H \approx 4{\cdot}7 \times 10^5$, $\tau_{cr} = 0{\cdot}029$; (a) $Ra = 8{\cdot}62 \times 10^4$, $t = 80$s, $\tau = 0{\cdot}043$; (b) $Ra = 1{\cdot}18 \times 10^5$, $t = 220$ s, $\tau = 0{\cdot}17$; (c) $Ra = 1{\cdot}30 \times 10^5$, $t = 420$ s, $\tau = 0{\cdot}224$; (d) $Ra = 1{\cdot}50 \times 10^5$, $t = 745$ s, $\tau = 0{\cdot}397$.

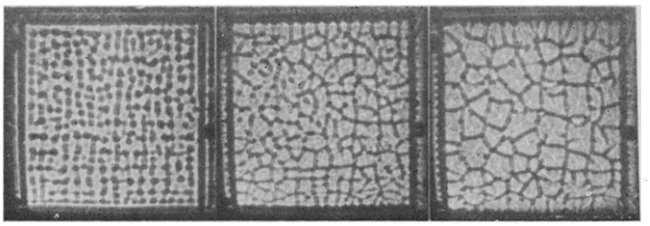

FIG. 15. "High heating rate"—5cs Oil, $d = 0{\cdot}01270$ m, $H \approx 1{\cdot}4 \times 10^6$, $\tau_{cr} = 0{\cdot}016$: (a) $Ra = 1{\cdot}82 \times 10^5$, $t = 45$ s, $\tau = 0{\cdot}024$; (b) $Ra = 2{\cdot}50 \times 10^5$, $t = 155$ s, $\tau = 0{\cdot}082$; (c) $Ra = 2{\cdot}74 \times 10^5$, $t = 310$ s, $\tau = 0{\cdot}165$.

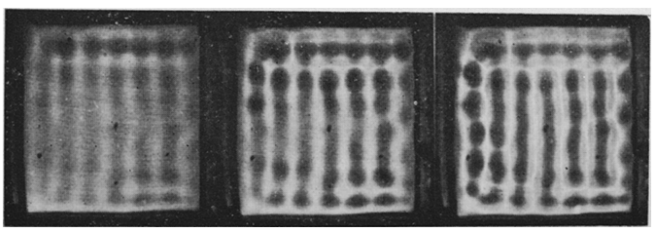

FIG. 16. "Intermediate heating rate"— 500cs Oil, $d = 0{\cdot}01905$ m, $H \approx 1{\cdot}3 \times 10^4$, $\tau_{cr} = 0{\cdot}217$: (a) $Ra = 5{\cdot}74 \times 10^3$, $t = 760$ s $\tau = 0{\cdot}229$; (b) $Ra = 5{\cdot}91 \times 10^3$, $t = 870$ s, $\tau = 0{\cdot}262$; (c) $Ra = 5{\cdot}8 \times 10^3$, $t = 1010$ s, $\tau = 0{\cdot}304$.

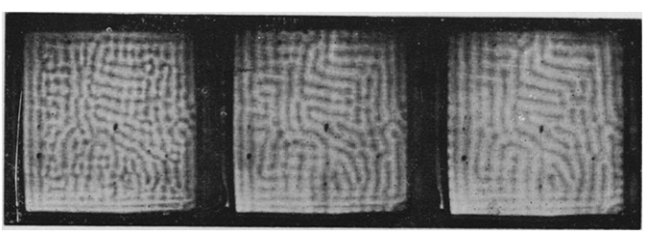

FIG. 17. "Intermediate heating rate"—5cs Oil, $d = 0{\cdot}00635$ m, $H \approx 1{\cdot}2 \times 10^4$, $\tau_{cr} = 0{\cdot}298$: (a) $Ra = 5{\cdot}78 \times 10^3$, $t = 195$ s, $\tau = 0{\cdot}42$; (b) $Ra = 6{\cdot}47 \times 10^3$, $t = 495$ s, $\tau = 1{\cdot}05$; (c) $Ra = 7{\cdot}49 \times 10^3$, $t = 970$ s, $\tau = 2{\cdot}07$.

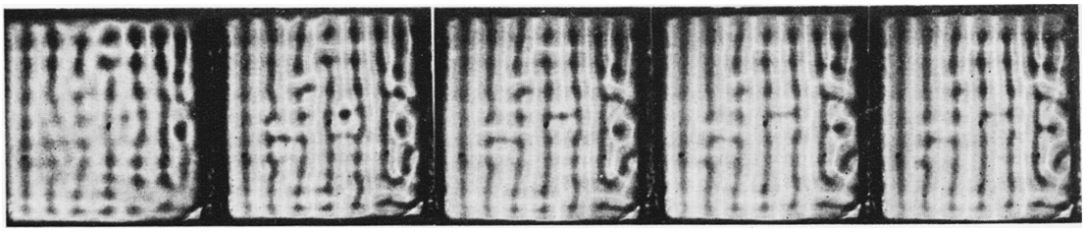

FIG. 18. "Intermediate heating rate"—100cs Oil, $d = 0{\cdot}01270$ m, $H \approx 1{\cdot}1 \times 10^4$, $\tau_{cr} = 0{\cdot}173$: (a) $Ra = 5{\cdot}08 \times 10^3$, $\tau = 380$ s, $\tau = 0{\cdot}263$; (b) $Ra = 5{\cdot}19 \times 10^3$, $t = 510$ s, $\tau = 0{\cdot}353$; (c) $Ra = 5{\cdot}12 \times 10^3$, $t = 710$ s, $\tau = 0{\cdot}491$; (d) $Ra = 5{\cdot}40 \times 10^3$, $t = 920$ s, $\tau = 0{\cdot}636$; (e) $Ra = 5{\cdot}43 \times 10^3$, $t = 1070$ s, $\tau = 0{\cdot}739$.

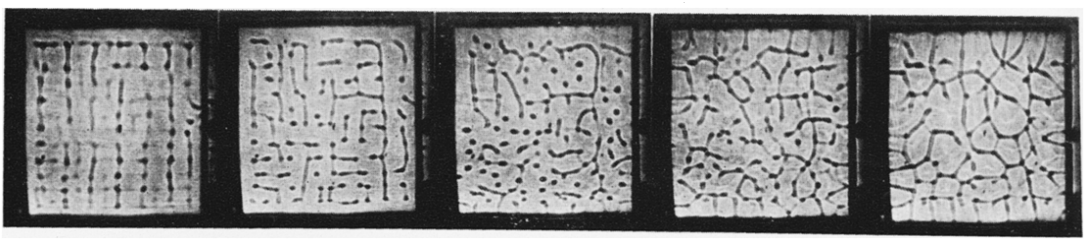

FIG. 19. "High heating rate"—5cs Oil, $d = 0{\cdot}01905$ m, $H \approx 1{\cdot}5 \times 10^6$, $\tau_{cr} = 0{\cdot}019$: (a) $Ra = 1{\cdot}79 \times 10^5$, $t = 95$ s, $\tau = 0{\cdot}022$; (b) $Ra = 2{\cdot}06 \times 10^5$, $t = 135$ s, $\tau = 0{\cdot}032$; (c) $Ra = 2{\cdot}38 \times 10^3$, $t = 205$ s, $\tau = 0{\cdot}048$; (d) $Ra = 2{\cdot}76 \times 10^5$, $t = 355$ s, $\tau = 0{\cdot}084$; (e) $Ra = 3{\cdot}24 \times 10^5$, $t = 610$ s, $\tau = 0{\cdot}144$.

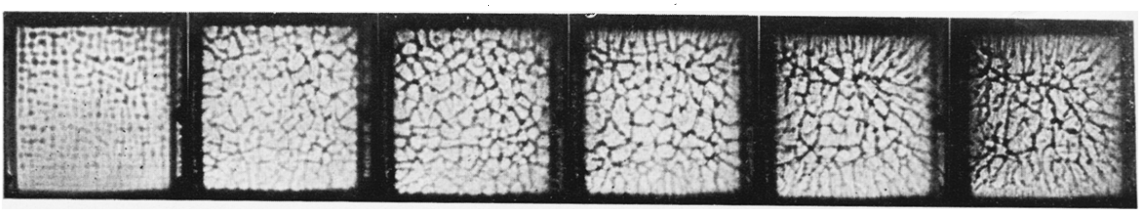

FIG. 20. "High heating rate"—5cs Oil, $d = 0{\cdot}01905$ m, $H \approx 1{\cdot}1 \times 10^7$, $\tau_{cr} = 0{\cdot}006$; (a) $Ra = 8{\cdot}01 \times 10^5$, $t = 35$ s, $\tau = 0{\cdot}008$; (b) $Ra = 1{\cdot}31 \times 10^6$, $t = 130$ s, $t = 0{\cdot}031$; (c) $Ra = 1{\cdot}53 \times 10^6$, $t = 250$ s, $\tau = 0{\cdot}059$; (d) $Ra = 1{\cdot}66 \times 10^6$, $t = 400$ s, $\tau = 0{\cdot}095$; (e) $\tau = 1{\cdot}76 \times 10^6$, $t = 595$ s, $\tau = 0{\cdot}140$; (f) $Ra = 1{\cdot}82 \times 10^6$, $t = 735$ s, $\tau = 0{\cdot}174$.

The heating rate and Rayleigh number of the next sequence (Fig. 19, $H \approx 1{\cdot}5 \times 10^6$) are close to those at which the photographs for Fig. 15 were taken when the plate spacing was only $\frac{1}{2}$ in. The development is markedly similar; the initial closed-cell pattern branches out to form short sections of rolls which eventually form a random set of polygonal cells. The last sequence shown (Fig. 20, $H \approx 1{\cdot}1 \times 10^7$) is taken at a higher heating rate of the series of experiments than any of the previous ones. Again the initial pattern is that of closed cells. A polygonal structure then develops similar to that observed in Fig. 19, and this then changes into a rather fine-grained structure which no longer exhibits any clearly defined polygons but now gives the definite impression of a turbulent motion.

In reviewing the photographic records as a whole, let us first examine the steady state patterns, which can be compared to those obtained by previous investigators. The present experiments extend up to Rayleigh numbers of about 2×10^6. At the lower portion of this range the steady state pattern would be formed by two dimensional rolls. For Rayleigh numbers of the order of 10^4–10^5 the flow could be characterized in terms of vermiculate rolls and irregular but steady polygonal cells. For the high Rayleigh number of the present series, irregular polygonal cells could still be seen but the flow was no longer steady; periodically columns of hot fluid would rise and would then merge with the boundaries of the cells, and the flow within the cellular boundaries gave the appearance of turbulent motion.

Of the observations made by previous investigators, the ones by Krishnamurti [21, 22] are among the most thorough. A comparison with the present findings shows that the two sets of results are quite comparable. The patterns observed by Krishnamurti at the various Rayleigh numbers are of the same type and character and may be described in the same terms.

As mentioned earlier, the present work was directed towards the transient phase, and it is of interest that a type of pattern occurred during this phase which had not been observed in the steady state. In fact, this pattern, which was described as "closed cells", was the initial pattern to appear for all heating rates. Occasional reference (e.g. Graham [23] and Spangenberg and Rowland [6]) has been made in the literature to a pattern in which the fluid "plunges" along individual columns. Such a flow has been mentioned, for example, in a free surface fluid layer which is cooled from above by evaporation. It could well be that this plunging motion may be identified with the "closed cell" pattern which has been observed so consistently as the initial pattern in the present series of experiments.

In the foregoing paragraphs an attempt was made to describe the observations in terms of certain typical flow patterns. Although it has been possible to characterize the flow in this manner, it should be repeated that one should not expect at present to be able to predict with any accuracy the shape of the flow patterns, the location of the flow elements, their relative orientation, etc. It is, in fact, an important feature of the flow in the present experiments, that the exact configurations are most sensitive to boundary conditions, slight non-uniformities in heating and similarly imperfectly controlled factors. On the other hand the *average* heat transfer coefficient (or Nusselt number) over the the plate as a whole is surprisingly little affected by these variants in the pattern, and the relation between Nusselt number and Rayleigh number (as given in Fig. 9, for example) may be considered generally applicable. In some cases, however, it may be important to predict the exact location of hot and cold regions, and this information cannot be derived from the available data. In this connection, it may be well to recall the famous picture of Bénard convection as presented by Bénard himself. This picture shows a beautiful and well defined pattern of identical hexagonal cells. It must be remembered, however, that this pattern was obtained for a very thin layer of fluid in which surface tension played a major role.

SUMMARY AND CONCLUDING REMARKS

The purpose of the present experiments was to study the transient phases of free convection in a plane fluid layer heated from below. The quantitative results could be presented in the form of graphs of the Nusselt number vs the Rayleigh number (Fig. 9). The region of transient convection has been marked on this graph. It is bounded on one side by the region in which the heat transfer is purely by conduction and on the other by the region in which the steady state conditions have been reached. At Rayleigh numbers below the critical the region of transient convection disappears, of course, as no motion will take place under these conditions. For high heating rates and correspondingly high Rayleigh numbers, the transient period between onset of convection and steady state increases. As a measure of its duration one might take the time from the onset of instability to the time when the Nusselt number has reached a value within, say 15 per cent, of that at the steady state. At a dimensionless heating rate of $H = 10^6$ this duration is equal to 0·035 in dimensionless terms. Using the conditions of $\varkappa = 0{\cdot}112 \times 10^{-6}\ \mathrm{m^2\,s^{-1}}$ and $d = 0{\cdot}1905$ m from the present experiments, this corresponded to an elapsed time of 3·16 h. As the dimensionless time has a factor of d^2 in the denominator actual times tend to be long for large size systems. For a system with properties equal to those sometimes mentioned (see Turcotte and Oxburgh [26]) for the earth mantle ($\varkappa = 10^{-6}\ \mathrm{m^2\,s^{-1}}$, $d = 1{\cdot}5 \times 10^6$ m) the above time interval would be $2{\cdot}5 \times 10^9$ years!

In addition to the quantitative results the development of the convective flow patterns was observed and photographic records were taken. In all cases the initial flow results in a pattern of more or less regularly spaced dots, which are believed to represent columns of rising hot fluid accompanied by a downward flow of cool fluid surrounding the columns. This pattern has been termed "closed cells" in the report and it may well represent the "plunging flow" which has been reported by some investigators. The final patterns develop fairly directly from the initial one. At lower Rayleigh numbers the final pattern tends towards two dimensional rolls; in the next higher range "vermiculate rolls" and "irregular polygons" develop; and at the highest Rayleigh numbers tested the flow inside the polygons takes on a turbulent character. All of these steady state patterns have been observed previously. Although the convective flow could be described in terms of certain patterns, it has to be realized that these patterns are not geometrically precise and the exact location of "rolls" and "cells" cannot be predicted with accuracy. This fact may be important in applications in which local heat transfer and flow conditions are of interest.

ACKNOWLEDGEMENTS

The work reported herein has been supported in part by the National Science Foundation (Grant No. GK-572). This support is gratefully acknowledged. One of the authors (R. C. Nielsen) also was awarded the John and Fannie Hertz Foundation Scholarship and would like to express his gratitude for this generous assistance.

REFERENCES

1. H. Bénard, Les tourbillons cellulaires dans une nappe liquide transportant de la chaleur par convection en regime permanent, *Ann. Chem. Phys.* **23**, 62–144 (1901).
2. S. Chandrasekhar, *Hydrodynamic and Hydromagnetic Stability*. Oxford University Press, Oxford (1961).
3. L. A. Segel, Non-linear hydrodynamic stability theory and its applications to thermal convection and curved flows, *Non-equilibrium Thermodynamics Variational Techniques and Stability*, edited by R. J. Donnelly, R. Herman and I. Prigogine, pp. 165–197. University of Chicago Press, Chicago (1966).
4. J. Brindley, Thermal convection in horizontal fluid layers, *J. Inst. Maths. Applics.* **3**, 313–343 (1967).
5. R. K. Soberman, Onset of convection in liquids subjected to transient heating from below, *Physics Fluids* **2**, 131–138 (1959).
6. W. G. Spangenberg and W. R. Rowland, Convective circulation in water induced by evaporative cooling, *Physics Fluids* **4**, 743–750 (1961).
7. T. D. Foster, Onset of convection in a layer of fluid cooled from above, *Physics Fluids* **8**, 1770–1774 (1965).
8. T. D. Foster, Onset of manifest convection in a layer of fluid with a time-dependent surface temperature, *Physics Fluids* **12**, 2482–2487 (1969).
9. L. M. Blair and J. A. Quinn, The onset of cellular convection in a fluid layer with time-dependent density gradients, *J. Fluid Mech.* **36**, 385–400 (1969).
10. E. G. Mahler and R. S. Schechter, The stability of a

fluid layer with gas absorption, *Chem. Engng Sci.* **25**, 955–968 (1970).
11. R. E. PLEVAN and J. A. QUINN, The effect of monomolecular films on the rate of gas absorption into a quiescent liquid, *A.I.Ch.E. Jl* **12**, 894–902 (1966).
12. K. ONAT and U. GRIGULL, The onset of convection in a horizontal fluid layer heated from below. *Wärme- und Stoffübertragung* **3**, 103–113 (1970).
13. R. E. KRISHNAMURTI, Finite amplitude thermal convection with changing mean temperature: the stability of hexagonal flows and the possibility of finite amplitude instability, Ph.D. dissertation, University of California, Los Angeles, California (1967).
14. R. E. KRISHNAMURTI, Finite amplitude convection with changing mean temperature, part 2: an experimental test of the theory, *J. Fluid Mech.* **33**, 457–463 (1968).
15. F. H. BUSSE and J. A. WHITEHEAD, Instabilities of convection rolls in a high Prandtl number fluid, *J. Fluid Mech.* **47**, 305–320 (1971).
16. A. W. GOLDSTEIN, Stability of a horizontal fluid layer with unsteady heating from below and time dependent body force, NASA Tech. Rep. R-4 (1959).
17. I. G. CURRIE, The effect of heating rate on the stability of stationary fluids, *J. Fluid Mech.* **29**, 337–347 (1967).
18. T. D. FOSTER, Stability of a homogeneous fluid cooled uniformly from above, *Physics Fluids* **8**, 1249–1257 (1965).
19. E. W. P. HAHNE, Natural convection heat transfer through an enclosed horizontal layer of supercritical carbon dioxide, *Wärme- und Stoffübertragung* **1**, 190–196 (1965).
20. R. C. NIELSEN, Transient heating in Bénard convection, Ph.D. dissertation, California Institute of Technology, Pasadena, California (1971).
21. H. T. ROSSBY, A study of Bénard convection with and without rotation, *J. Fluid Mech.* **36**, 309–335 (1969).
22. D. AVSEC, Tourbillons thermoconvectifs dans l'air application à la météorologie. Publ. Sci. et Techn. du Ministère de l'Air Nr. 155, Paris (1939).
23. R. E. KRISHNAMURTI, On the transition to turbulent convection, part 1: the transition from two-to-three-dimensional flow, *J. Fluid Mech.* **42**, 295–307 (1970).
24. R. E. KRISHNAMURTI, On the transition to turbulent convection, part 2: the transition to time-dependent flow, *J. Fluid Mech.* **42**, 309–320 (1970).
25. A. GRAHAM, Shear patterns in an unstable layer of air, *Phil. Trans.* **232A**, 285–296 (1933).
26. D. L. TURCOTTE and E. R. OXBURGH, Finite amplitude convective cells and continental drift, *J. Fluid Mech.* **28**, 29–42 (1967).

TRANSFERT THERMIQUE TRANSITOIRE EN CONVECTION DE BENARD

Résumé—On présente des résultats expérimentaux relatifs au chauffage variable en fonction du temps pour la convection de Bénard avec des huiles de silicone dont la viscosité est égale à 5, 100 et 500 centistoke. Les épaisseurs de la couche fluide sont 0,00635m, 0,0127m et 0,01905m. Dans chaque essai le flux thermique à la surface inférieure est aproximativement constant et dans plusieurs essais on couvre la gamme $9{,}2\ 10^2$ à $1{,}9\ 10^7$ pour les flux (en terme adimensionnel). Les expériences ont été conduites pour étudier les effets de différentes vitesses de chauffage sur le déclenchement de la convection, sur la variation du nombre de Rayleigh avec le temps et sur le développement du mouvement. Des observations sont faites sur des clichés photographiques par méthode des ombres. Lorsque le flux thermique à la surface inférieure est augmenté, la différence de température nécessaire à l'initiation de la convection croît tandis que le temps d'établissement du mouvement décroît. Dans les conditions de ces essais on observe en premier une configuration en "cellule fermée" peu après la mise en mouvement. Cette configuration n'apparait pas dans l'état permanent. A cause du "grand" nombre de Prandtl (supérieur à 100) il est suffisant, pour caractériser l'état de la couche fluide, de préciser le temps et le flux thermique à la face inférieure.

INSTATIONÄRER WÄRMEÜBERGANG BEI BÉNARD KONVEKTION

Zusammenfassung—Es werden experimentelle Ergebnisse einer Untersuchung über den Einfluss der zeitabhängigen Heizung auf die Bénard-Konvektion besprochen. Als Fluid wurde Silikonöl mit den Viskositäten 5, 100 und 500 CS verwendet. Die untersuchten Schichthöhen betrugen dabei 0,00635 m, 0,01270 m und 0,01905 m. Während eines Versuchs war der Wärmestrom an der unteren Oberfläche näherungsweise konstant, und in verschiedenen Versuchen variierte dieser Wärmestrom von $9{,}2.10^2$ bis $1{,}9.10^7$ (in dimenssionsloser Darstellung). Zweck der Experimente war es, den Einfluss unterschiedlicher Wärmeströme auf den Beginn der Konvektion, auf die Änderung der Rayleigh-Zahl mit der Zeit und auf die Entwicklung der Konvektionsbewegung zu untersuchen.

Die Beobachtung erfolgte durch Fotografieren von Schattenbildern. Wenn der Wärmestrom an der unteren Oberfläche zunimmt steigt auch die für das Einsetzen der Konvektion notwendige Temperaturdifferenz an, während die Zeitspanne bis zum Einsetzen der Konvektion abnimmt. Unter den vorliegenden Bedingungen wird nach dem Einsetzen der Konvektion eine "geschlossene Zellstruktur" beobachtet. Diese Struktur tritt im stationären System nicht auf. Wegen der "hohen" Prandtl-Zahl (grösser als 100) ist die Angabe der Zeit und des Wärmestroms zur Beschreibung des Zustands der Fluid-Schicht ausreichend.

НЕСТАЦИОНАРНЫЙ ТЕПЛООБМЕН ПРИ КОНВЕКЦИИ БЕНАРА

Аннотация—Представлены экспериментальные результаты по исследованию влияния нестационарного нагрева на конвекцию Бенара. В качестве жидкости использовалось кремнеорганическое масло со знаучениями вязкости 5, 100 и 500 сст. (сантистокс). Толщина слоев жидкости составляла 0,00635; 0,01270 и 0,01905 м. В каждом опыте тепловой поток на нижней поверхности был приблизительно постоянным, а в ряде опытов диапазон изменения потока тепла составлял $9.210^2 \div 1.910^7$ (в безразмерных величинах). В экспериментах ставилась задача выяснить влияния различных скоростей нагрева на возникновение конвекции, изменение значения числа Рэлея и на развитие конвективного движения. Наблюдения за конвекцией производились с помощью теневой фотографии. По мере увеличения теплового потока на нижней поверхности разность температур, необходимая для возникновения конвекции, увеличивалась, а характерное время (до возникновения конвекции) уменьшалось. В условиях данного эксперимента вскоре после возникновения конвективного движения первой наблюдается картина «замкнутой ячейки». Такая картина не возникает с стационарном состоянии. Ввиду большого значения числа Прандтля (более чем 100) для описания состояния слоя жидкости достаточно определить характерное время и значение теплового потока на нижней поверхности.